The sequence and crystal structure of the alpha-amino acid ester hydrolase from Xanthomonas citri define a new family of beta-lactam antibiotic acylases

Barends, Thomas; Polderman - Tijmes, Jolanda; Jekel, PA; Hensgens, CMH; de Vries, Erik; Janssen, DB; Dijkstra, Bauke W.

Published in:
The Journal of Biological Chemistry

DOI:
10.1074/jbc.M302246200

Publication date:
2003

THE JOURNAL OF BIOLOGICAL CHEMISTRY
Vol. 278, No. 25, Issue of June 20, pp. 23076–23084, 2003

Printed in U.S.A.

The Sequence and Crystal Structure of the α-Amino Acid Ester Hydrolase from *Xanthomonas citri* Define a New Family of β-Lactam Antibiotic Acylases*

Received for publication, March 4, 2003, and in revised form, April 4, 2003
Published, JBC Papers in Press, April 8, 2003, DOI 10.1074/jbc.M302246200

Thomas R. M. Barends‡§, Jolanda J. Polderman-Tijmes§¶‖, Peter A. Jekel¶, Charles M. H. Hensgens‡, Erik J. de Vries¶, Dick B. Janssen¶, and Bauke W. Dijkstra‡ ‡‡**

From the Departments of ‡Biophysical Chemistry and ¶Biochemistry, Groningen Biomolecular Sciences and Biotechnology Institute, University of Groningen, Nijenborgh 4, NL-9747 AG Groningen, The Netherlands

α-Amino acid ester hydrolases (AEHs) catalyze the hydrolysis and synthesis of esters and amides with an α-amino group. As such, they can synthesize β-lactam antibiotics from acyl compounds and β-lactam nuclei obtained from the hydrolysis of natural antibiotics. This article describes the gene sequence and the 1.9-Å resolution crystal structure of the AEH from *Xanthomonas citri*. The enzyme consists of an α/β-hydrolase fold domain, a helical cap domain, and a jellyroll β-domain. Structural homology was observed to the *Rhodococcus* cocaine esterase, indicating that both enzymes belong to the same class of bacterial hydrolases. Docking of a β-lactam antibiotic in the active site explains the substrate specificity, specifically the necessity of an α-amino group on the substrate, and explains the low specificity toward the β-lactam nucleus.

β-Lactam antibiotics form a large family of widely applied antibacterials. Most of them are derived from a handful of naturally occurring antibiotics like penicillin G, penicillin V, and cephalosporin C by replacing their acyl groups with synthetic ones. Initially, this was achieved by chemical means but at present, enzymatic methods are preferred (1). A well known enzyme used for these conversions is penicillin acylase (EC 3.5.1.11) from *Escherichia coli*. This enzyme is used both for the production of the β-lactam nucleus 6-aminopenicillanic acid (6-APA)[1] by cleaving off phenylacetic acid from penicillin G and for the coupling of new acyl groups to 6-APA or other β-lactam nuclei. Penicillin acylase is, however strongly inhibited by its product phenylacetic acid (2), which must therefore be removed before coupling of a new acyl group to the β-lactam nucleus can take place. In addition, β-lactam nuclei are not very stable at the alkaline pH optimum of penicillin acylase.

By contrast, α-amino acid ester hydrolases (AEHs) do not have these disadvantages. These enzymes catalyze the hydrolysis and synthesis of esters and amides of α-amino acids exclusively, and do not attack the amide bond of a β-lactam. They can be used to acylate a β-lactam using an ester as acyl donor, as shown in Fig. 1. Because the AEHs require an α-amino group on the substrate, they are not inhibited by phenylacetic acid (3). Together with their ability to accept various β-lactam nuclei without cleaving them, this makes them suitable for generating widely used antibiotics such as ampicillin, amoxicillin, and the cephalosporins cephadroxil and cephalexin. The slightly acidic pH optimum of AEH, which is beneficial for β-lactam stability, is another advantage of AEHs for biocatalytic applications, as is their stereospecificity toward the acyl donor (4).

One of the first AEHs that was isolated and characterized is the enzyme from *Xanthomonas citri* (5–11). This enzyme was found to be a homotetramer with subunits of 72 kDa (6). Kinetic studies indicated the occurrence of an acyl-enzyme intermediate in the hydrolysis and acylation reactions of β-lactam antibiotics (3, 7, 12).

This article reports the gene and 1.9-Å resolution crystal structure of the AEH from *X. citri*. The structure is the first in this family of β-lactam antibiotic acylases. The catalytic domain consists of the well known α/β-hydrolase fold, with a classical catalytic triad. The *X. citri* AEH structure highlights a peculiar active site, in which a classical Ser-His-Asp catalytic triad is combined with unusual features like a rare oxyanion hole composed of a main chain amide and a tyrosine side chain, and a cluster of negatively charged residues, which is likely involved in substrate recognition. Genetic comparisons show the conservation of these features that allows the structural definition of a novel family of serine hydrolases.

EXPERIMENTAL PROCEDURES

Materials—Antibiotics and related compounds were provided by DSM Life Sciences (Delft, The Netherlands). Oligonucleotides for cloning of the AEH-encoding gene were provided by Eurosequence (Groningen, The Netherlands). Chemicals used in DNA manipulation procedures were purchased from Roche Diagnostics GmbH (Mannheim, Germany) and used as recommended by the manufacturer. DNA sequences were determined at the Department of Medical Biology of the University of Groningen.

Bacterial Strains, Plasmids, and Growth Conditions—*X. citri* IFO 3835 was grown for 16 h at 28 °C in a 10-liter fermentor on the medium described by Takahashi *et al.* (5) with the addition of 0.005% (w/v) $FeSO_4$. *E. coli* strains HB101 (13) and the methionine-deficient strain *E. coli* B834(DE3) (Novagen Inc., Madison, WI) were used for cloning derivatives of pEC (DSM Life Sciences). *E. coli* XL1 Blue MR (Stratagene, La Jolla, CA) was the host for a genomic library of *X. citri* in the cosmid pWE15 (Amp^R) (Stratagene). For production of the selenomethionine-incorporated protein, *E. coli* B834(DE3) carrying the construct

* This work was supported in part by The Netherlands Foundation for Chemical Research (CW) with financial aid from The Netherlands Foundation for Scientific Research (NWO) and the Dutch Ministry of Economic Affairs (Senter). The costs of publication of this article were defrayed in part by the payment of page charges. This article must therefore be hereby marked "*advertisement*" in accordance with 18 U.S.C. Section 1734 solely to indicate this fact.

§ Both authors contributed equally to this work.
‖ Supported by DSM Life Science Products, The Netherlands.
** Current address: Mucovax BV, Niels Bohrweg 11–13, NL-2333 CA Leiden, The Netherlands.
‡‡ To whom correspondence should be addressed. Tel.: 31-50-3634381; Fax: 31-50-3634800; E-mail: B.W.Dijkstra@chem.rug.nl.

[1] The abbreviations used are: 6-APA, 6-amino penicillanic acid; AEH, α-amino acid ester hydrolase; MES, 4-morpholineethanesulfonic acid; 7-ACA, 7-aminocephalosporanic acid.

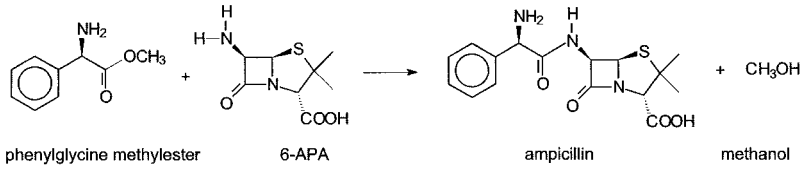

FIG. 1. **Transacylation reaction catalyzed by α-amino acid ester hydrolases, resulting in antibiotic formation.** As an example, the synthesis of ampicillin from D-phenylglycine methylester and 6-APA is shown. The AEHs can also hydrolyze antibiotics, cleaving them at the amide bond to the side chain, not at the lactam bond.

pXc (see below) was grown for 30 h at 30 °C on M9 medium (14) supplemented with a vitamin and spore solution (15), DL-selenomethionine (100 mg/liters), chloramphenicol (34 mg/liters), and isopropyl-β-D-thiogalactopyranoside (0.4 mM).

Isolation of α-Amino Acid Ester Hydrolase from X. citri and Amino Acid Sequence Determination—The α-amino acid ester hydrolase from *X. citri* was purified essentially as described for the *Acetobacter turbidans* AEH (16). For sequence analysis of *X. citri* AEH, ~100 μg of protein was sliced from a SDS-PAGE gel and digested with trypsin. From the digest, those peptides containing a tryptophan (high absorbance at 297 nm) were selected for sequencing. Eurosequence BV (Groningen, The Netherlands) carried out further preparation of the sample and determined the amino acid sequence by automated Edman degradation (model 477A, Applied Biosystems).

Preparation and Screening of the X. citri Genomic Library—The gene encoding the AEH from *X. citri* (*aehX*) was cloned from a genomic DNA cosmid library via Southern blotting. To this end, genomic DNA from *X. citri* was isolated and partially digested with *Sau*3A as described before (16). The conditions were optimized to obtain fragments of 30–45 kb. These were ligated in cosmid pWE15 (Amp^r), which had been digested with *Bam*HI and dephosphorylated with alkaline phosphatase. *In vitro* packaging and infection of *E. coli* XL1 Blue MR was carried out according to the recommendations of the manufacturer of the DNA packaging kit (Roche Diagnostics). Part of the gene encoding *X. citri* AEH was cloned by PCR amplification from chromosomal DNA using two primers based on the determined internal amino acid sequences, pF, 5′-AAYCCNAGYGARGTNGAYCAYGC-3′, and pR, 5′-YTTRTGCCACCANGGNARYTGYTC-3′ (Y is T or C; R is A or G; N is any base). The PCR product was isolated from gel (QiaQuick kit, Qiagen, GmbH, Hilden, Germany), cloned, and sequenced. A gene probe for the *aehX* gene was made using matching primers based on the DNA sequence of the PCR fragment. The forward primer was 5′-ACCGATGCCTGGGACACC-3′(upstream of pF) and the reverse primer was 5′-CAGGCCTGCGGCCTTGGC-3′ (downstream of pR). These primers were used to amplify a 317-bp fragment with *Taq* polymerase using the PCR DIG probe synthesis mixture from Roche Diagnostics. To obtain the whole gene, colony hybridization with the cosmid library was carried out as described by Polderman-Tijmes *et al.* (16) using the specific probe.

Cloning of aehX into an Expression Host—For expression of *aehX* in *E. coli*, it was placed under control of a *tac* promotor in the pEC vector (17), resulting in pXc. For cloning in the *Nde*I/*Hin*dIII site of pEC the gene was amplified with the primers, 5′-TCCGGAGTC<u>ATTA</u>**ATG**CGCCGCCTTGCCAC-3′ (*Asn*I site underlined, start codon in bold) and a reverse primer, 5′-ACCGGTGCC<u>AAGCTT</u>**TCA**ACGTTACCGGCAG-3′ (*Hin*dIII site underlined, stop codon in bold). After denaturation of the DNA (pWE15 (*aehX*)) amplification was performed in 30 cycles of 30 s at 94 °C, 1 min at 58 °C, and 1 min and 30 s at 72 °C. Product and vector were both subjected to restriction, and subsequently ligated. The ligation mixture was used to transform *E. coli* HB101.

Enzyme Assays and Determination of Kinetic Constants—AEH activities were routinely measured by incubating purified *X. citri* AEH with a substrate at varying concentrations in 50 mM phosphate buffer, pH 7.0, at room temperature. The hydrolysis products were analyzed by high performance liquid chromatography (18). Cephalexin hydrolysis was measured in a concentration range from 0.95 to 15 mM; ampicillin from 0.5 to 15 mM; phenylglycine methylester from 4 to 250 mM; 4-hydroxyphenylglycine methylester from 0 to 30 mM; amoxicillin from 0.5 to 15 mM; cefatrizine from 0.3 to 15 mM. Cephadroxil, phenylacetic acid methylester, and penicillin G were all used at 10 mM, but phenylglycine at 40 mM.

Two potential inhibitors were tested by following their effect on the hydrolysis of 50 mM phenylglycine methylester in 50 mM sodium phosphate, pH 6.2. A 0.1 M stock solution of 2,4-dinitrobenzenesulfenyl chloride was made in 50 mM sodium phosphate, pH 7.0. Phenylmethylsulfonyl fluoride was dissolved at 0.1 M in methanol. 2,4-Dinitrobenzenesulfenyl chloride was used at 1 mM with 400 nM enzyme (70-kDa monomer), whereas the effect of phenylmethylsulfonyl fluoride was evaluated at 4 mM with 10–20 nM enzyme (final concentrations). The effects of the solvents were measured separately and used to correct the inhibitory effects.

Isolation of Recombinant Selenomethionine-incorporated X. citri α-Amino Acid Ester Hydrolase from E. coli—Selenomethionine-AEH was purified from *E. coli* B834(DE3) (pXc) cells grown in the presence of 100 mg/liter DL-selenomethionine. The selenomethionine-incorporated enzyme was purified as described above with the addition of 5 mM dithiothreitol to all buffers to prevent oxidation of the selenium. The enzyme was concentrated to 5 mg/ml in 20 mM cacodylate buffer, pH 6.5, by ultrafiltration (YM30, Amicon).

Crystallization—Protein crystals were grown essentially as described earlier (19). Briefly, 1.5 μl of concentrated *X. citri* AEH was mixed with an equal volume of 12–15% PEG 8000 in 0.1 M cacodylate, pH 6.5, and equilibrated against 500 μl of this precipitant solution. Prior to freezing, crystals were briefly soaked in 15% PEG 8000 in 0.1 M MES, pH 6.5, to remove the arsenic-containing cacodylate, as arsenic has spectral properties comparable with those of selenium that interfere with MAD data collection around the selenium wavelength. Crystals were cryoprotected by soaking for a few seconds in 25% glycerol, 15% PEG 8000 in 0.1 M MES, pH 6.5.

Data Collection and Structure Determination—A three-wavelength MAD dataset was collected to 2.5-Å resolution from a crystal of selenomethionine-labeled protein at the BW7A beamline of the EMBL outstation at the DESY synchrotron in Hamburg, Germany. Also, 80% complete native data to 1.8 Å were collected at the ID14-2 beamline of the ESRF in Grenoble, France. Additionally, a 1.9-Å resolution dataset was collected at the BW7B beamline at DESY, Hamburg. All data were processed with the HKL package (20). Using the peak wavelength data of the MAD dataset, 62 selenium sites could be identified using the program Shake-and-Bake (21) with standard settings (22). These sites were refined against the full three-wavelength MAD dataset using the program SOLVE (23), which was also used for the calculation of phases. Solvent flattening was performed with RESOLVE (24), resulting in an electron density map of excellent quality. The resolution was extended to 1.8 Å using ARP/wARP (25) and the incomplete data from ID14-2, after which the autotracing option in wARP (26) built 98% of the structure. No averaging was applied at any stage.

Refinement and Model Building—Refinement was performed using the program REFMAC5 (27) against the 1.9-Å data from BW7B, without using a σ cutoff. No NCS was imposed at any stage. The current model contains 2452 amino acids, 1806 water molecules, four calcium ions, and nine glycerol molecules. Rebuilding was done with XtalView (28). Docking of ampicillin in the active site was done with Quanta (Accelrys) and CNS (29).

RESULTS AND DISCUSSION

The AEH Family of β-Lactam Antibiotic Acylases—The gene for the α-amino acid ester hydrolase from *X. citri* encodes a polypeptide of 637 amino acids with a calculated molecular weight of 70,915. A BLAST search (30) with the deduced amino acid sequence revealed an identical sequence, annotated as a glutaryl 7-ACA acylase, from *Xanthomonas axonopodis* pv. *citri* strain 306 (protein ID number AAM37193) (31). Other proteins with high sequence identities (93, 78, 62, and 61%, respectively) are the putative glutaryl 7-ACA acylases from *Xanthomonas campestris* pv. *campestris* strain ATCC 33913 (protein ID number AAM41516 (31), *Xylella fastidiosa* (protein ID number AAF83839), and *Zymomonas mobilis* (protein ID number AAD29644), and the α-amino acid ester hydrolase from *A. turbidans* (protein ID number AF439262 (16)). Lower sequence identities (28%) were found with the glutaryl 7-ACA acylase

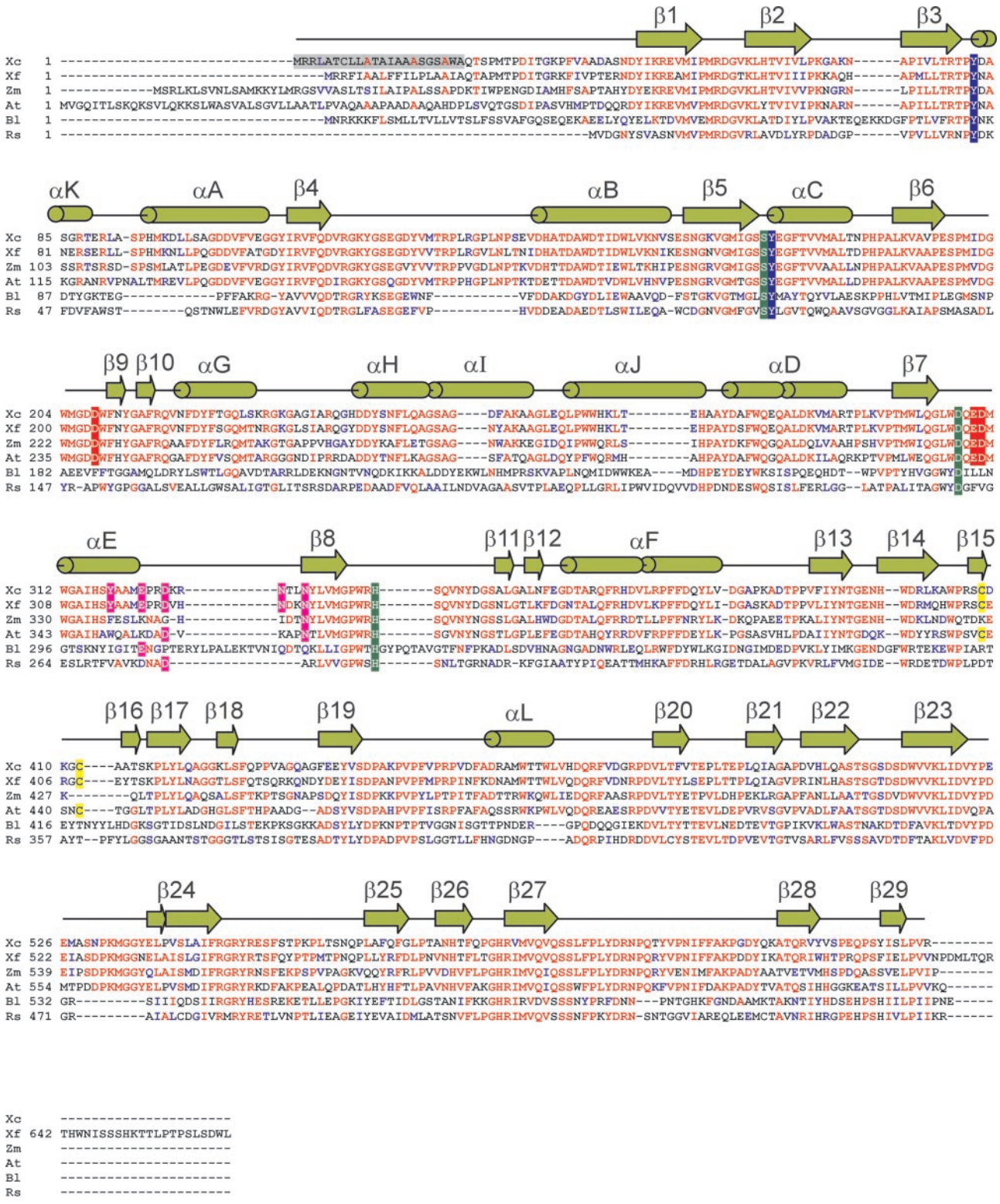

FIG. 2. **Sequence alignment of members of the proposed family of AEHs from *X. citri* (*Xc*) and *A. turbidans* (*At*), *X. fastidiosa* (*Xf*), and *Z. mobilis* (*Zm*), the 7-ACA glutaryl acylase from *B. laterosporus* (*Bl*), and the cocaine esterase from *Rhodococcus* sp. (*Rs*).** A *green box* indicates the catalytic triad residues, a *blue box* those forming the oxyanion hole, and a *red box* the residues involved in binding the α-amino moiety. Residues binding the calcium are surrounded by a *purple box*, and the cysteines forming the disulfide bridge by a *yellow box*. The *gray box* shows the putative N-terminal leader peptide.

from *Bacillus laterosporus* (protein ID number BAA10148 (32)) and cocaine esterase cocE from *Rhodococcus* sp. (protein ID number AAF42807 (33)) of which the structure has been published (34). A sequence alignment of the proteins from *X. citri*, *X. fastidiosa*, *Z. mobilis*, *A. turbidans*, *B. laterosporus*, and *Rhodococcus* sp. is shown in Fig. 2. No sequence similarity to any known β-lactam antibiotic acylase other than the *B. laterosporus* glutaryl 7-ACA acylase was found, supporting the hypothesis that the AEHs constitute a new family of β-lactam antibiotic acylases, which contains the proteins from the *Xanthomonas* strains, *A. turbidans*, *X. fastidiosa*, and *Z. mobilis*.

TABLE I
Data collection and refinement statistics

$R_{sym} = \Sigma_{hkl} \Sigma_i |I_{hkl,i} - I_l| / \Sigma_{hkl} \Sigma_i I_{hkl,i}$ for the intensity I of i observations of reflection h. R-factor = $\Sigma |F_{obs} - F_{calc}| / \Sigma F_{obs}$ (F_{obs} = observed structure factor, F_{calc} = calculated structure factor). R_{free} = R-factor calculated with 5% of randomly chosen data that were omitted from the refinement. Values in parentheses are for the highest resolution shell.

Data collection	Dataset				
	Selenomethionine MAD on BW7A			ID14–2	BW7B
	Peak	Inflection	Remote		
Wavelength (Å)	0.9779	0.9783	0.9392	0.933	0.846
Space group		$P2_1$		$P2_1$	$P2_1$
Unit cell					
a		89.80		89.98	89.77
b		125.86		125.78	126.02
c(Å)		132.14		132.08	132.29
β(°)		91.0		90.9	90.94
Resolution (Å)	2.35	2.35	2.25	1.80	1.90
Observations	1,873,199	1,872,141	1,067,980	1,742,445	1,307,283
Unique reflections	99721	97017	99732	205579	220969
Completeness (%)	99.7 (96.9)	99.7 (96.8)	99.6 (95.8)	81.4 (45.3)	95.6 (95.8)
R_{sym}	0.074 (0.183)	0.057 (0.178)	0.061 (0.195)	0.077 (0.378)	0.055 (0.210)
Refinement					
Resolution range (Å)					129–1.9
Reflections used					209646
Protein atoms					19392
Water molecules					2246
Glycerol molecules					11
Calcium ions					4
R-factor					0.149
R-factor highest resolution shell (1.900-1.949 Å)					0.211
R_{free}					0.178
R_{free} highest resolution shell (1.900-1.949 Å)					0.242
Root mean square deviations					
Bonds (Å)					0.013
Angles (°)					1.143
Ramachandran plot					
Most favored regions (%)					87.4%
Allowed (%)					12.3%
Disallowed (%)					0.3%

Quaternary Structure—X. citri AEH was overproduced in selenomethionine-labeled form and crystallized as described before (19). Phases were obtained using multiwavelength anomalous dispersion, and the model was built almost entirely through automated methods. The structure was refined to crystallographic and free R-factors of 14.9 and 17.8%, respectively, at a resolution of 1.9 Å. Data and model statistics are shown in Table I.

The asymmetric unit was found to contain a tetramer, which is approximately spherical, with a diameter of ~100 Å (Fig. 3*A*). A tetrameric arrangement is in agreement with gel filtration and ultracentrifugation studies of the *X. citri* AEH by Kato *et al.* (6). The four monomers form an approximate tetrahedron and enclose a large water-filled space with two large entrances. All four active sites (see below) are on the inside of the tetramer, facing the water-filled space and are accessible only through these entrances. The four monomers are virtually identical, their Cα atoms superimposing to within 0.2 Å.

The N terminus of each molecule is observed from Thr-24 onwards. From Thr-24, the polypeptide forms a 40-Å long "arm" (residues 24–44) that lies on the surface of an adjacent monomer. This monomer, in turn, places its N-terminal arm onto the first monomer. Thus, the tetramer is composed of two dimers of which each monomer donates its N terminus to the other molecule of the same dimer. The large entrances to the central cavity lie between these two arms. The interaction of the two monomers in the dimer buries a surface of ~3700 Å^2, almost all of which is because of interactions involving the arms. The interacting surfaces of a monomer with the monomers of the other dimer within the tetramer measure ~2,100 and ~1,100 Å^2. In total, ~14,000 Å^2 are buried by inter-monomer contacts within the 280-kDa tetramer. Several of these contacts are formed by hydrogen bonds, involving both main chain and side chain atoms.

Monomer Structure—The monomer (Fig. 3*B*) consists of an N-terminal α/β-hydrolase fold (35) with large insertions, and a C-terminal domain that consists largely of β-strands with a jellyroll topology, with extra elements of secondary structure in the crossover loops.

The α/β-hydrolase fold domain consists of a central, mostly parallel β-sheet of 10 β-strands, flanked on either side by α-helices (Fig. 4*A*). The second strand runs antiparallel to the others. Like in other α/β-hydrolases (35), the twist in the central sheet is large, with a difference in orientation of the first and the last strand of about 90 degrees. At the end of the fifth strand, a very tight turn into a helix contains Ser-174, which is thus observed in the common position for the nucleophile in α/β-hydrolase fold enzymes. As usual in α/β-hydrolases (36), this residue adopts an unfavorable main chain conformation (ϕ = 64.9°, φ = −119.3°, averaged over all four monomers). A loop protruding from strand β3 (residues 82 to 101) covers strands β1, β2, and β4 of the central β-sheet and approaches the connection between the N-terminal arm and strand β1 (Fig. 4*A*). The polypeptide chain continues into helix αA (residues 105–109) that contacts strand β4. The predominantly helical cap domain (residues 199–278, Fig. 4*B*) connects strand β6 and helix αD as is usual in α/β-hydrolase enzymes. From strand β6, a loop (residues 199–209) extends into a small two-stranded antiparallel β-sheet (strand β9, residues 210 and 211 and strand β10, residues 214–215) followed by helices αG (220–227), αH (243–250), αI (253–259), and αJ (266–273). The chain continues into helix αD (residues 279–291), which flanks the central sheet. Between strand β8 and helix αF, a β-hairpin turn (strands β11 and β12, residues 349–350 and 353–354, respectively) is formed. After helix αF, an additional two

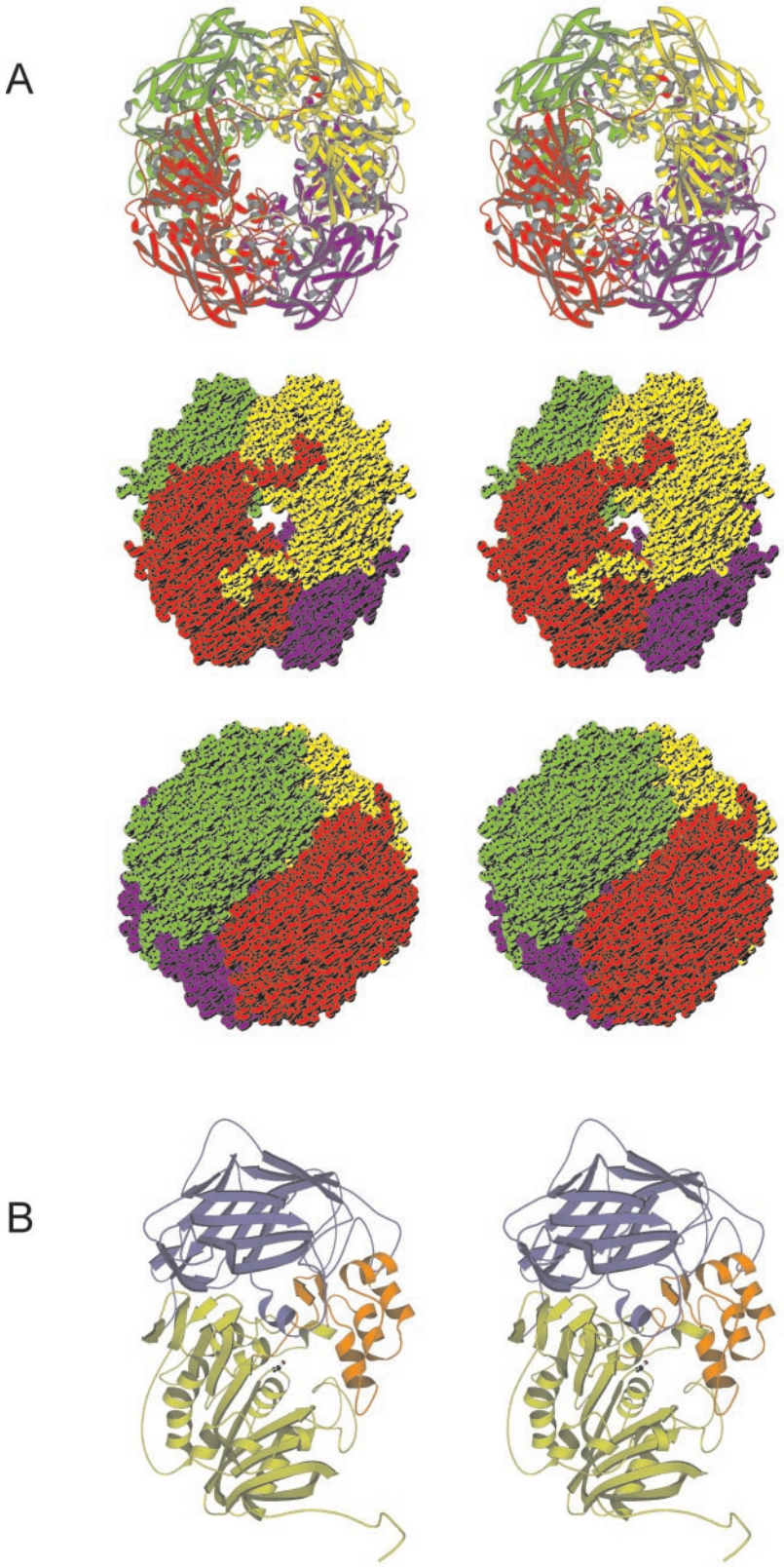

FIG. 3. *A*, stereo representation of the *X. citri* AEH tetramer, looking through the large entrance into the central cavity. Each monomer is individually colored. The figure was prepared using Molscript (45). *B*, stereo representation of the *X. citri* AEH monomer. The α/β-hydrolase fold domain is colored *green*, the cap domain *orange*, and the C-terminal jellyroll domain *blue*. The catalytic Ser-174 is shown in ball-and-stick representation. The figure was prepared using Molscript (45).

strands are seen at the end of the central β-sheet, strand β13 (parallel, residues 388–392), and strand β14 (antiparallel, residues 397–401).

The C-terminal domain adopts a jellyroll fold, which is connected to the α/β-hydrolase domain via a small linker, which is tightened into a compact structure by a disulfide bond between Cys-408 and Cys-412. The hydrogen bonding pattern is broken at the edges of the two antiparallel β-sheets of the jellyroll (strands β17, 18, 22, 25, 29, and β20, 23, 24, and 27) such that a β-sandwich rather than a β-barrel is formed. In the crossover loops, two small antiparallel two-stranded β-sheets are formed (strands β19/β28 and β21/β26), closing the β-sandwich of the jellyroll on either side to create a box-like structure. Two insertions project away from this box. The first insertion (residues 446–481) contains an α-helix, which comes into close proximity of the active site and may thus play a role in catalysis. The other

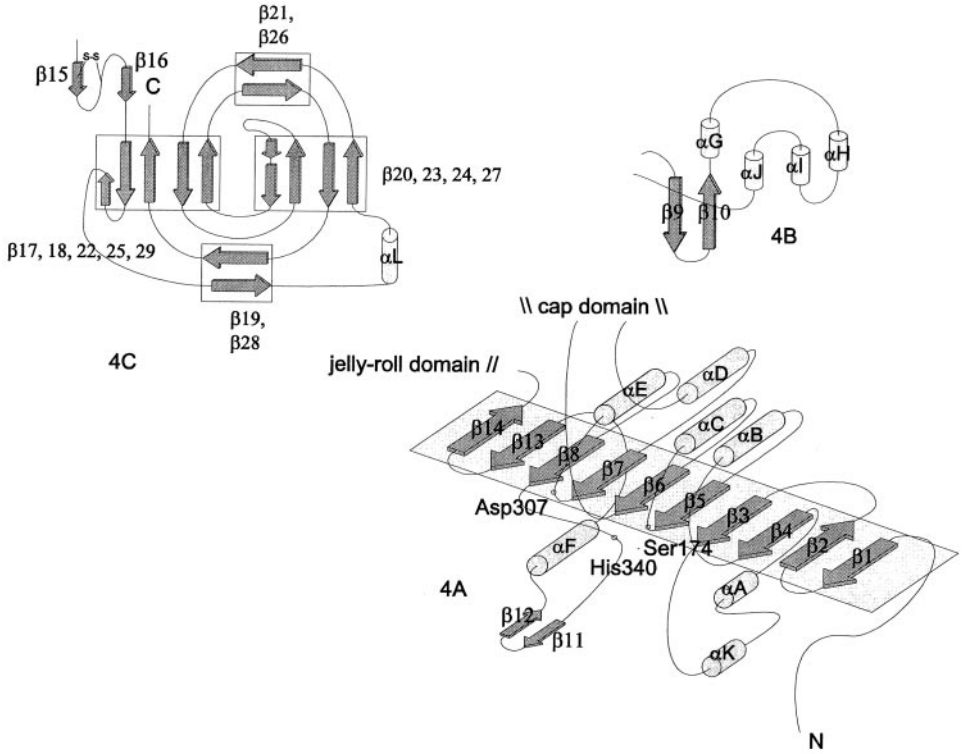

FIG. 4. **Topology diagrams of the different domains in *X. citri* AEH.** *A*, α/β-hydrolase fold domain (residues 24–205 and 286–404). *B*, the mainly α-helical cap domain (residues 206–284). *C*, the jellyroll domain (residues 405–637) with two large insertions and several smaller insertions. The disulfide bond between Cys-408 and Cys-412 is indicated.

insertion (residues 525 to 535) makes contacts with two other monomers and contributes to tetramer formation.

The fold of the monomer resembles that of the cocaine esterase from *Rhodococcus* sp. (cocE) of which the structure was previously published (34). The structures can be superimposed to a root mean square difference of 2.3 Å for 390 corresponding Cα atoms. Whereas the α/β-hydrolase and jellyroll domains are similar, differences are observed in the cap domain and the insertions in the jellyroll domain. The cap domain of cocE is larger, extending into the region where the entrance to the tetramer is found in *X. citri* AEH. Arranging four cocE molecules in a way similar to the AEH tetramer shows that the entrances to the central cavity would be severely blocked by the larger cap domains of cocE. More recently, the structure of the *Lactococcus lactis* X-prolyl dipeptidyl aminopeptidase PepX was published, which exhibits the same three-domain fold and organization as AEH and cocE, apart from an additional N-terminal domain involved in oligomerization (37), like the N-terminal arms in AEH.

A Novel Calcium Binding Site Structurally Distinct from the EF-hand—On the surface of the tetramer and opposite the active site, a metal ion is bound by the side chains of Glu-322, Asp-325, Asn-328 (through its O-δ), and the main chain carbonyl oxygen of Asn-331. It is further coordinated by two water molecules, one of which is hydrogen bonded to the hydroxyl group of Tyr-318. This results in a pentagonal-bipyramidal coordination sphere consisting of only oxygen atoms. The ion was modeled as a calcium ion. Refinement of the structure with a magnesium ion in this position was unsatisfactory because it yielded unrealistically low B-factors for the ion. All coordinating amino acids stem from the same loop (Fig. 5), which connects helix αE with strand β8. This is in contrast to the situation in EF-hands, where the calcium binding loop is found between two helices. In *X. citri* AEH, the coordinating residues (*X*) form an *X*··*X*··*X*··*X* motif (Fig. 2) in which every third residue coordinates the ion, again in contrast to the EF-hand case

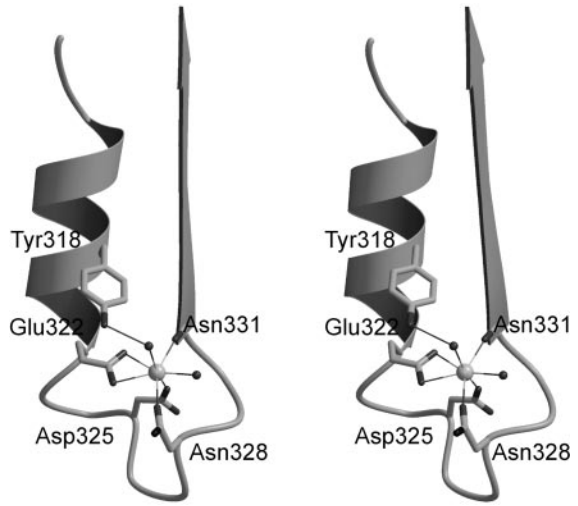

FIG. 5. **Stereo figure of the calcium binding motif.** The coordinating residues are indicated. The figure was prepared using Bobscript (46) and Raster3D (47).

(*X*·*X*·*X*·*X*·*X*··*X*) (38). This binding motif is therefore distinctly different from the EF-hand and represents a novel calcium ion binding motif. Sequence alignment of the proteins from *X. citri*, *A. turbidans*, *X. fastidiosa*, *B. laterosporus*, and *Z. mobilis* shows this motif to be present only in the *X. citri* and *X. fastidiosa* sequences. The calcium binding motif is also not observed in cocE.

Active Site Structure—The catalytic Ser-174 is found on the "nucleophilic elbow" between strand β5 and helix αC. Its position in this narrow turn places it near the N-terminal end of the 10-residue long helix C, which can stabilize negative charges through its helix dipole (35). Ser-174 is roughly in the middle of a distinct active site pocket. It is in close contact with His-340, which in turn is hydrogen bonded to Asp-307. These

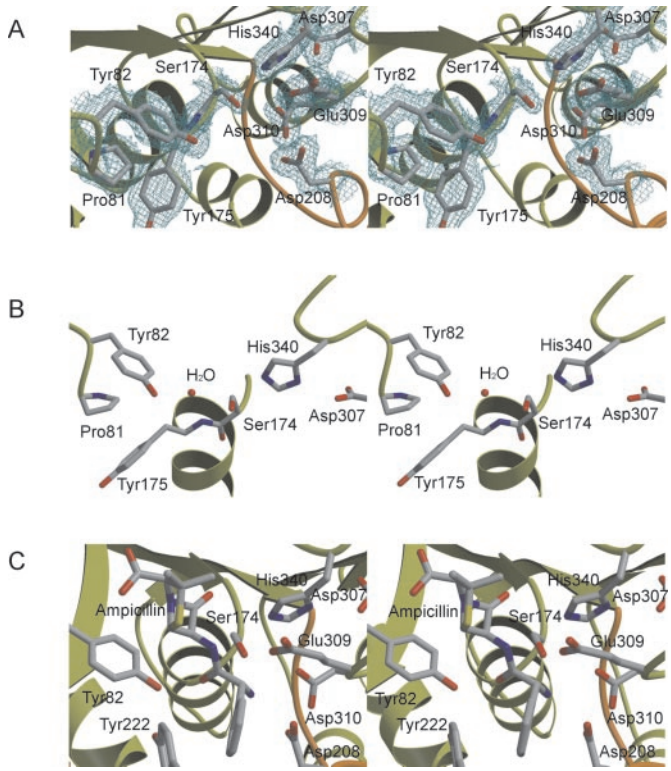

FIG. 6. **The active site of AEH.** *A*, stereo representation of the active site of *X. citri* AEH. The residues involved in binding and catalysis are shown. The main chain trace is colored according to the domain architecture (*green*, α/β-hydrolase domain; *orange*, cap domain). The σ_A-weighted $2F_o - F_c$ electron density map is contoured at 1.2 σ. *B*, close-up of the residues of the catalytic triad, and those forming the oxyanion hole. The water molecule occupying the oxyanion hole is also shown. *C*, stereo figure of the model of ampicillin binding to *X. citri* AEH. The figure was prepared using Bobscript (46) and Rasterd3D (47).

residues constitute a catalytic triad (Fig. 6, *A* and *B*) and are found in the canonical positions in the sequence (36): Ser-174 on the turn between strand β5 and helix αC, His-340 on the linker between strand β8 and helix αF, and Asp-307 between strand β7 and helix αE. The orientation of the His-340 N-δ is unfavorable for hydrogen bond formation with the Ser-174 O-γ, but a 10° rotation around the His-340 χ_1 could remedy this.

In many catalytic triads of serine hydrolases, a hydrogen bond-like interaction is observed between the His C-ϵ and a backbone carbonyl group. This interaction has been proposed by Derewenda *et al.* (39) to stabilize the positively charged imidazolinium intermediate developing during catalysis. However, in the case of AEH, the distance between the His-340 C-ϵ and the nearest backbone carbonyl (of Ser-198) is too large (3.9 Å) for this interaction to have much effect. On the other hand, the His-340 C-ϵ is just 3 Å away from the Asp-310 O-δ, which might perform the proposed stabilizing function. However, the imidazole ring and the Asp-310 carboxylate moiety are far from coplanar. We therefore believe that this interaction is a not a hydrogen bond as such, but that it can stabilize the imidazolinium ion through Coulomb interactions.

In α/β-hydrolases, the backbone amide of the residue directly following the catalytic nucleophile stabilizes the ionic intermediate by forming part of an oxyanion hole. In the case of *X. citri* AEH, a water molecule is observed close to the backbone NH of Tyr-175 (Fig. 6*B*), in the position expected for the oxyanion. An additional contribution to the stabilization of the oxyanion could be made by the side chain hydroxyl group of Tyr-82, which forms a hydrogen bond with the water molecule.

The architecture of the oxyanion hole (Fig. 6*B*) is identical to that observed in cocE and PepX. Apart from these enzymes, the only other enzyme known to use a tyrosine side chain in oxyanion stabilization is prolyl oligopeptidase. Is has been noted (40–42) that because of the lower pK_a of tyrosine side chains, they could be more capable of oxyanion stabilization than the backbone or side chain amides used for this purpose in other enzymes. Furthermore, enzymes in which a side chain contributes to the oxyanion hole are ideal enzymological model systems because the oxyanion hole can be easily modified by site-directed mutagenesis (41–43).

Next to the catalytic histidine, a cluster of carboxylate groups protrudes into the active site (Fig. 6*A*). This cluster is formed by Asp-208, Glu-309, and Asp-310. Glu-309 and Asp-310 are in the loop that connects strand β7 and helix αE, whereas Asp-208 is part of the loop between strand 6 and the cap domain. A survey of homologous genes shows that these residues are absolutely conserved among the proteins from the proposed family of AEHs (Fig. 2), but are not present in the *B. laterosporus* glutaryl acylase or the *Rhodococcus* sp. cocaine esterase. Consequently, this cluster of acidic residues may be crucial to the α-amino acid ester hydrolase function. A characteristic of this function is the importance of the α-amino group of the substrate, which is obvious from Table II. Substrates without an α-amino group, such as penicillin G and phenylacetic acid methylester are not hydrolyzed by *X. citri* AEH. Also, the broadly active serine hydrolase inhibitor phenylmethylsulfonyl fluoride, which does not contain an amino group, did not appreciably inhibit *X. citri* AEH (90% residual activity). Furthermore, it has been shown that the enzyme has a preference for the positively charged form of the amino-containing substrates (3). Given the position of Asp-208, Glu-309, and Asp-310, close to the catalytic Ser-174 residue, it is conceivable that these residues are responsible for the recognition of the α-amino group of the substrate and would thus constitute a structural feature of major importance for the function of the enzyme.

The proximity of the side chains of Asp-208, Glu-309, and Asp-310 in the active site would lead to an energetically unfavorable clustering of negatively charged atoms requiring stabilization. One way in which the enzyme stabilizes the clustering of negative charge is through a hydrogen bond of the O-ϵ of Glu-309 with the N-ϵ of Trp-465, which is conserved in the AEHs of the *Xanthomonas* strains, *X. fastidiosa*, *A. turbidans*, and *Z. mobilis*. Trp-465 is part of the helical insertion in the jellyroll domain (residues 448–481), which is located close to the carboxylate cluster. The importance of a tryptophan residue for activity is corroborated by the reduction in activity of the enzyme (65% residual activity) in the presence of 2,4-dinitrobenzenesulfenyl chloride, which reacts with tryptophan residues.

Together with the high sequence homology, the conservation of the residues forming the carboxylate cluster in the putative acylases from *X. fastidiosa* and *Z. mobilis* identifies these proteins as AEHs, in contrast with their previous annotations as 7-ACA glutaryl acylases. On the other hand, the absence of these residues in the *B. laterosporus* sequence makes it unlikely that the latter protein is an AEH.

Modeling of Substrate in the Active Site—To visualize how the cluster of Asp-208, Glu-309, and Asp-310 could recognize the α-amino group of the substrate, we have manually docked an ampicillin molecule into the active site based on the positions of the catalytic serine, the oxyanion hole, and the negatively charged cluster (Fig. 6*C*). The amide bond of ampicillin was placed close to the nucleophilic Ser-174, with the amide oxygen in the oxyanion hole, making hydrogen bonds to the backbone amide of Tyr-175 and the phenolic OH of Tyr-82.

TABLE II
Kinetic parameters of AEH from X. citri

Substrate	K_M	k_{cat}	k_{cat}/K_M
	mM	s^{-1}	$s^{-1}\ mM^{-1}$
D-Phenylglycine amide	ND[a]	1.6	
D-Phenylglycine methylester	90	1860	21
D-4-Hydroxyphenyl-glycine methylester	—[b]	—	9[c]
Ampicillin	1.2	58	48
Amoxicillin	—	—	2[c]
Cephalexin	1.8	160	89
Cephadroxil	—	ND	
Cefatrizine	<1	2.3	>2.3
Phenylacetic acid methylester	—	ND	
Penicillin G	—	ND	

[a] ND, no conversion detected. Measured at 50 mM.
[b] —, not determined.
[c] Determined from the linear part of the Michaelis-Menten curve.

The α-amino group could then be positioned to make electrostatic interactions with the cluster of carboxylates formed by Asp-208, Glu-309, and Asp-310. To remove unfavorable contacts, a short energy minimization was carried out in which only the ampicillin molecule was allowed to move. In the resulting model, aromatic ring stacking interactions occur between the aromatic ring of phenylglycine and Tyr-222. Furthermore, the model predicts a stacking interaction between the phenylglycine ring and the side chain of Asp-208. The side chains of Met-200, Trp-209, and Asp-219 further delimit the pocket binding the phenyl ring. These residues belong to the cap domain, which shows a large degree of structural and functional variation within the α/β-hydrolase family (36). In the structurally related cocaine esterase, the cap domain binds the acyl group of the ester, which is consistent with our model. Because AEHs differ in their selectivity toward various antibiotics with substituted phenyl rings, differences in sequence would be expected in the regions just described.

The model predicts few interactions with the β-lactam nucleus, although stacking interactions with Tyr-82 seem likely. In addition to this, some polar residues extend into the space where the β-lactam is located. The relative paucity of interactions with the β-lactam nucleus is consistent with the fact that both penicillin- and cephalosporin-derived nuclei can bind.

Conclusions and Implications—We present here the first structure of an α-amino acid ester hydrolase. The *X. citri* AEH structure shows a peculiar spherical tetrameric state, which would only allow enzymatic action toward small molecules.

The *X. citri* AEH monomer displays a three-domain fold consisting of an α/β-hydrolase fold domain, a cap domain, and a C-terminal domain with a jellyroll fold. Within the active site, a canonical Ser-His-Asp catalytic triad is observed, but an interesting cluster of acidic residues close to the catalytic histidine sets the enzyme apart from other serine esterases. Given the remarkable specificity for substrates with a charged ammonium group, it is likely that this "carboxylate cluster" is responsible for recognition and binding of this group, as illustrated by molecular modeling. The conservation of this cluster, furthermore, allows the definition of an AEH family at the genetic level, distinguishing the AEHs from structurally related esterases and peptidases.

Acknowledgments—We thank Renske Heyman for the preparation of the *X. citri* genomic library and Ehmke Pohl for assistance with MAD data collection. We acknowledge the EMBL Hamburg outstation and the ESRF in Grenoble for synchrotron beam time, and the European Union for support of the work at the EMBL, Hamburg, through the HCMP Access to Large Installations Project.

REFERENCES

1. Bruggink, A., and Roy, P. D. (2001) in *Synthesis of β-Lactam Antibiotics* (Bruggink, A., ed) pp. 12–56, Kluwer Academic Publishers, Dordrecht
2. Alkema, W. B. L., Floris, R., and Janssen, D. B. (1999) *Anal. Biochem.* **275,** 47–53
3. Blinkovsky, A. M., and Markaryan, A. N. (1993) *Enzyme Microb. Technol.* **15,** 965–973
4. Fernandez-Lafuente, R., Hernández-Justiz, O., Mateo, C., Terreni, M., Alonso, J., Garcia-López, J. L., Moreno, M. A., and Guisan, J. M. (2001) *J. Mol. Catal. B Enzym.* **11,** 633–638
5. Takahashi, T., Yamazaki, Y., Kato, K., and Isona, M. (1972) *J. Am. Chem. Soc.* **94,** 4035–4037
6. Kato, K., Kawahara, K., Takahashi, T., and Kakinuma, A. (1980) *Agric. Biol. Chem.* **44,** 1069–1074
7. Kato, K. (1980) *Agric. Biol. Chem.* **44,** 1083–1088
8. Kato, K., Kawahara, K., Takahashi, T., and Kakinuma, A. (1980) *Agric. Biol. Chem.* **44,** 1075–1081
9. Hyun, C. K., Kim, J. H., and Ryu, D. D. Y. (1993) *Biotechnol. Bioeng.* **42,** 800–806
10. Hyun, C. K., Choi, J. H., and Kim, J. H. (1993) *Biotechnol. Bioeng.* **41,** 654–658
11. Rhee, D. K., Lee, S. B., Rhee, J. S., Ryu, D. D., and Hospodka, J. (1980) *Biotechnol. Bioeng.* **22,** 1237–1247
12. Nam, D. H., Kim, C., and Ryu, D. D. Y. (1985) *Biotechnol. Bioeng.* **27,** 953–960
13. Boyer, H. W., and Roulland-Dussiox, D. (1969) *J. Mol. Biol.* **41,** 459–472
14. Sambrook, J., Fritsch, E. F., and Maniatis, T. (1989) *Molecular Cloning: A Laboratory Manual*, 2nd Ed., Cold Spring Harbor Laboratory, Cold Spring Harbor, NY
15. Janssen, D. B., Scheper, A., and Witholt, B. (1984) in *Innovations in Biotechnology* (Houwink, E. H., and van der Meer, R. R., eds) Elsevier, Amsterdam, The Netherlands
16. Polderman-Tijmes, J. J., Jekel, P. A., Merode, V. A., Floris, T. A. G., van der Laan, J.-M., Sonke, T., and Janssen, D. B. (2002) *Appl. Environ. Microbiol.* **68,** 211–218
17. Alkema, W. B. L., Hensgens, C. M. H., Kroezinga, E. H., Vries de, E., Floris, R., van der Laan, J.-M., Dijkstra, B. W., and Janssen, D. B. (2000) *Protein Eng.* **13,** 857–868
18. Polderman-Tijmes, J. J., Jekel, P. A., Jeronimus-Stratingh, C. M., Bruins, A. P., van der Laan, J. M., Sonke, T., and Janssen, D. B. (2002) *J. Biol. Chem.*
19. Barends, T. R. M., Hensgens, C. M. H., Polderman-Tijmes, J. J., Jekel, P. A., de Vries, E. J., Janssen, D. B., and Dijkstra, B. (2003) *Acta Crystallogr. Sect. D Biol. Crystallogr.* **59,** 158–160
20. Otwinowksi, Z., and Minor, W. (1997) in *Macromolecular Crystallography, Part A* (Carter, C. W., Jr., and Sweet, R. M., eds) Vol. 276, pp. 307–326, Academic Press, New York
21. Smith, G. D., Nagar, B., Rini, J. M., Hauptmann, H. A., and Blessing, R. H. (1998) *Acta Crystallogr. Sect. D Biol. Crystallogr.* **54,** 799–804
22. Howell, P. L., Blessing, R. H., Smith, G. D., and Weeks, C. M. (2000) *Acta Crystallogr. Sect. D Biol. Crystallogr.* **56,** 604–617
23. Terwilliger, T. C., and Berendzen, J. (1999) *Acta Crystallogr. Sect. D Biol. Crystallogr.* **55,** 849–861
24. Terwilliger, T. C. (1999) *Acta Crystallogr. Sect. D Biol. Crystallogr.* **55,** 1863–1871
25. Van Asselt, E. J., Perrakis, A., Kalk, K. H., Lamzin, V. S., and Dijkstra, B. W. (1998) *Acta Crystallogr. Sect. D Biol. Crystallogr.* **54,** 58–73
26. Perrakis, A., Morris, R., and Lamzin, V. S. (1999) *Nat. Struct. Biol.* **6,** 458–463
27. Murshudov, G. N., Vagin, A. A., and Dodson, E. J. (1997) *Acta Crystallogr. Sect. D Biol. Crystallogr.* **53,** 240–255
28. McRee, D. E. (1999) *J. Struct. Biol.* **125,** 156–165
29. Brunger, A. T., Adams, P. D., Clore, G. M., DeLano, W. L., Gros, P., Grosse-Kunstleve, R. W., Jiang, J.-S., Kuszweski, J., Nilges, N., Pannu, N. S., Read, R. J., Rice, L. M., and Simonson, T., and Warren, G. L. (1998) *Acta Crystallogr. Sect. D Biol. Crystallogr.* **54,** 905–921
30. Altschul, S. F., Madden, T. L., Schäffer, A. A., Zhang, J., Zhang, Z., Miller, W., and Lipman, D. J. (1997) *Nucleic Acids Res.* **25,** 3389–3402
31. da Silva, A. C. R., Ferro, J. A., Reinach, F. C., Farah, C. S., Furian, L. R., Quaggio, R. B., Monteiro-Vitorello, C. B., Van Sluys, M. A., Almeida, N. F., Alves, L. M. C., do Amarai, A. M., and Kitajima, J. P. (2002) *Nature* **417,**

459–463
32. Aramori, I., Fukagawa, M., Tsumura, M., Iwami, M., Ono, H., Kojo, H., Kohsaka, M., Ueda, Y., and Imanaka, H. (1991) *J. Bacteriol.* **173,** 7848–7855
33. Bresler, M. M., Rosser, S. J., Basran, A., and Bruce, N. C. (2000) *Appl. Environ. Microbiol.* **66,** 904–908
34. Larsen, N. A., Turner, J. M., Stevens, J., Rosser, S. J., Basran, A., Lerner, R. A., Bruce, N. C., and Wilson, I. A. (2001) *Nat. Struct. Biol.* **9,** 17–21
35. Ollis, D. L., Cheah, E., Cygler, M., Dijkstra, B. W., Frolow, F., Franken, S. M., Harel, M., Remington, S. J., Silman, I., Schrag, J., Sussman, J. L., Verschueren, K. H. G., and Goldman, A. (1992) *Protein Eng.* **5,** 197–211
36. Nardini, M., Ridder, I. S., Rozeboom, H. J., Kalk, K. H., Rink, R., Janssen, D. B., and Dijkstra, B. W. (1999) *J. Biol. Chem.* **274,** 14579–14586
37. Rigolet, P., Mechin, I., Delage, M.-M., and Chich, J.-F. (2002) *Structure Fold. Des.* **10,** 1383–1394
38. Kretsinger, R. H. (1976) *Annu. Rev. Biochem.* **45,** 239–266
39. Derewenda, Z. S., Derewenda, U., and Kobos, P. M. (1994) *J. Mol. Biol.* **241,** 83–93
40. Fülop, V., Bocskei, Z., and Polgar, L. (1998) *Cell* **94,** 161–170
41. Szeltner, Z., Renner, V., and Polgár, L. (2000) *Prot. Sci.* **9,** 353–360
42. Turner, J. M., Larsen, N. A., Basran, A., Barbas, C. F., III, Bruce, N. C., Wilson, I. A., and Lerner, R. A. (2002) *Biochemistry* **41,** 12297–12307
43. Bryan, P., Pantoliano, M. W., Quill, S. G., Hsiao, H.-Y., and Poulos, T. (1986) *Proc. Natl. Acad. Sci. U. S. A.* **83,** 3743–3745
44. Carter, P., and Wells, J. A. (1990) *Proteins Struct. Funct. Genet.* **7,** 335–342
45. Kraulis, P. (1991) *J. Appl. Crystallogr.* **24,** 946–950
46. Esnouf, R. M. (1997) *J. Mol. Graph.* **15,** 133–138
47. Merrit, E. A., and Bacon, D. J. (1997) *Methods Enzymol.* **277,** 505–524